Study of microstructure, hydrogen solubility and corrosion of Ta-modified Zr-1Nb alloys for nuclear applications

Ferreirós, P.A.; Savoy Polack, E.C.; Lanzani, L.A.; Alonso, P.R.; Quirós, D.P.; Mieza, J.I.; Zelaya, E.; Knowles, Sandy; Rubiolo, G.H.

DOI:
10.1007/978-3-030-92381-5_129

Study of microstructure, hydrogen solubility and corrosion of Ta-modified Zr-1Nb alloys for nuclear applications

P.A. Ferreirós[a,b,c*], E.C. Savoy Polack[b], L.A. Lanzani[b], P.R. Alonso[b], D.P. Quirós[b], J.I. Mieza[b], E. Zelaya[d], A.J. Knowles[a], G.H. Rubiolo[b,c]

[a] School of Metallurgy and Materials, University of Birmingham, Birmingham, B15 2TT, UK.
[b] Gerencia Materiales (GAEN) - Comisión Nacional de Energía Atómica (CNEA), Instituto Sabato - Universidad Nacional de San Martín (UNSAM), Av. Gral. Paz 1499, San Martín, Buenos Aires B1650KNA, Argentina.
[c] Consejo Nacional de Investigaciones Científicas y Técnicas (CONICET), Godoy Cruz 2290, C1425FQB Ciudad Autónoma de Buenos Aires, Argentina
[d] CAB, Bustillo Ave. 9500, 8400, Bariloche, Argentina. CONICET.

Keywords: Zr-Nb alloys, Ta addition, phase transformation, corrosion, hydrogen solubility

Abstract

Modified Zr-1Nb alloys with Ta additions is a potential strategy to improve structural alloys for nuclear reactors. The effects of Ta on microstructural stability and resistance to corrosion of Zr–1Nb alloys were systematically investigated and elucidated. The $(\alpha + \beta)$ microstructure in Zr-1.05Nb, Zr-0.85Nb-0.20Ta and Zr-0.85Nb-0.40Ta (wt.%) alloys were obtained with the following two thermo mechanical processes after a water quenching from β*Zr*: a) annealed at 570 °C for 3840 h and b) a combination of intermediate annealing temperatures and cold rolled steps. Quantitative EDS-TEM analysis together with DSC measurements were used to characterise the changes in phase compositions and the fraction of beta-phase precipitates. Hydrogen solubility was measured in alloys with the first annealed condition. The Ta additions increase the monotectic transformation temperature, improves the steam corrosion at 400 °C and 10 MPa up to 14 days, and decreases slightly the hydrogen solubility. The higher thermal microstructural stability compared to Ta-free Zr-1Nb alloys provide potential advantages for increases in operating temperature or acceleration of precipitation kinetics during thermomechanical processing.

1. Introduction

The Zr-1Nb alloy is being used as an advanced cladding material for French pressurized water reactors (PWR), under the designation M5, and for similar application in Russian reactors under the designation E110. The absence of Sn in their chemical composition significantly improves corrosion and hydrogen-pickup resistance in high burnup [1]. Their corrosion resistance is known to increase when equilibrium particles of β_{Nb} phase (very rich in Nb) are present instead of the metastable β_{Zr} phase (19 wt% Nb) [2,3,4]. In recent studies by Moorehead et al. [5] is demonstrated that β_{Zr} precipitates dissolve faster than β_{Nb} precipitates therefore, the latter are more effective in retaining Nb and retarding the growth of the oxide layer. Since the corrosion tests for the different microstructures of the same alloy were carried out simultaneously in a single aqueous corrosive environment, the change in chemical activity of the various species due to the change in the thermodynamic equilibrium of the phases shows a magnitude able to produce a significant change in the corrosion behavior of this kind of alloy [6]. With these ideas in mind and thinking about to increase the corrosion resistance in the Zr-1Nb alloy, this study intent to add a third alloying element expecting that the two-phase microstructure $(\alpha_{Zr} + \beta_{Nb})$ remains and that the third atoms also tend to form the β_{Nb} precipitate. If the third alloying element increases the enthalpy of formation of the β_{Nb} precipitate, the activity of Nb and the third element also increases in the α_{Zr} matrix and therefore the dissolution kinetic of both phases to form the oxide will decrease.

Tantalum is a promising minor alloying element for doping in Zr-Nb alloys. The only published work on the ternary system Zr-Ta-Nb [7], with data in the Zr apex, reports the stability of the biphasic microstructure below the monotectoid temperature of the Zr-Nb binary system (620 °C). However, viewed from the material selection philosophy for nuclear fuel cladding, the thermal neutron absorption cross section of Ta (20.6 barns) is too high [8].

(*) Corresponding author: p.ferreiros@bham.ac.uk (P.A. Ferreirós). Postal address: Engineering North Campus, School of Metallurgy & Materials, Elms Road, University of Birmingham, Edgbaston, Birmingham, B15 2TT, United Kingdom.

Still, the neutron economics of replacing Nb with Ta in the Zr-1Nb alloy for use in the cladding material must be evaluated. The increase of the macroscopic thermal neutron absorption cross section of the alloy can be compensated decreasing the thickness of the cladding if there is a yield stress increase due to solid solution hardening.

The work presented herein attempts to answer in part these questions and elucidate if Ta addition to Zr-1Nb alloy is to be favorably considered in the future alloy development.

2. Experimental Methods

The three alloys used in this study were processed from 25 g button melted in an electric arc furnace with a tungsten electrode and a water-cooled copper crucible in an argon atmosphere. Zr Sponge (68 ± 16 ppm Hf, 148 ± 24 ppm Fe, 628 ± 63 ppm O, 30 ± 4 ppm N and 45 ± 1.5 ppm H), Nb and Ta elements with purity better than 99.9 wt% were used. The buttons were turned and remelted several times to promote chemical homogeneity. In the melting process, weight losses of less than 0.04 % were obtained. Their nominal compositions were: Zr-1.05Nb [(98.9485 ± 0.0004)Zr, (1.052 ± 0.039)Nb]; Zr-0.85Nb-0.20Ta [(98.9483 ± 0.0003)Zr, (0.851 ± 0.032)Nb, (0.201 ± 0.032)Ta] and Zr-0.85Nb-0.40Ta [(98.7510 ± 0.0004)Zr, (0.850 ± 0.035)Nb, (0.399 ± 0.035)Ta].

The arc-melted buttons were beta-solution treated at 1100 °C for 30 min and followed by a water quenching (β_{Zr} quenched). To prevent oxidation, the buttons were wrapped in a tantalum foil and encapsulated into a quartz tube which was evacuated and backfilled with argon.

The alloy buttons were sectioned parallel to their axis of revolution to extract a coupon approximately 3 cm long and 1.5 cm wide from the central part of each button for further rolling process. The two remaining parts of the button were used to reach the formation of secondary precipitate phases (SPP) from the β_{Zr} quenched condition by isothermal annealing at 570 °C up to 3840 h. After the annealing, one of these parts was used for metallurgical characterization while the other provided two solid cylinders of approximately ϕ 3.5 x 5.6 mm for differential scanning calorimetry (DSC) and a sheet of approximately 108 mm^2 in area and 1 mm thick for corrosion testing.

The quenched coupon was 60% hot-rolled after a pre-heating at 570 °C for 30 min, annealing 3 hours at 570 °C in vacuum and 50% cold-rolled two times to a final thickness of 0.8 mm. Between the cold rolling steps, the sheet was annealed at 570 °C for 3 h in vacuum. The grain microstructure after the rolling sequence was observed with the aid of an optical microscope and polarized light. Several test samples were removed from the rolled alloys sheet, ϕ 3.5 mm disc type sample for DSC analysis and 10 mm side rectangular prism type for corrosion testing.

The final arrangement of the SPP in the microstructure of alloys was studied by light microscopy using brightfield-darkfield contrast and scanning electron microscopy (SEM) using secondary electron mode. The examined surfaces were metallographically prepared by polishing with abrasive paper up to grade 600 and etching with 10HF-45HNO_3-45$C_3H_8O_3$ (vol.%) by swabbing for 25 seconds. In each alloy that has reached the state of thermodynamic equilibrium at 570 °C after the β_{Zr} quenched condition, the microstructures were also examined using a transmission electron microscope (TEM) equipped with an energy dispersive X-ray spectrometer (EDS). Selected area diffraction patterns (SADP) were obtained and analyzed to determine the crystal structure of the SPP and, the chemical compositions of the phases were quantitatively measured by the EDS-TEM technique using Zr-Nb, Zr-Ta and Nb-Ta experimental Cliff-Lorimer sensitivity factors from standard alloys [9]. Matrixes were measured on thin films and the SPP on carbon extractive replicas.

The transformation temperature and the dissolution enthalpy of the SPP in each thermomechanical condition of the alloy was determined from high sensitivity differential scanning calorimetry (DSC) measurements with a heating rate of 5 °C/min under an Ar dynamic atmosphere. In addition, the dissolution enthalpy of the β_{Nb} phase obtained with each alloy that has reached the state of thermodynamic equilibrium at 570 °C was used as a calibration standard to quantify the global mass fraction of the β_{Nb} phase present in the rolled alloys [10].

Hydrogen solubility was measured only in the alloy materials that has reached the thermodynamic equilibrium state at 570 °C. The second ϕ 3.5 ×5.6 mm cylindrical sample of each alloy was subjected to the charge of hydrogen gas in a Sievert-type equipment to increase its hydrogen concentration by 200 wt ppm. The incorporation of hydrogen in each sample was carried out at 550 °C under a high purity hydrogen atmosphere at a pressure around 10 Torr. The dissolution and precipitation temperature (TSSD and TSSP, respectively) of zirconium hydrides were determined with the DSC method. The thermal cycle was a heat up ramp from room temperature up to 500 °C, a hold-time of 10 min and then a cooldown ramp to room temperature [11]. The heating and cooling rates were 10 °C /min.

Specimens for corrosion testing were mechanically ground up to 1200 grit SiC paper, and then pickled with a solution of 50 vol.% deionized water + 47 vol.% HNO3 + 3 vol.% HF. After this, they were rinsed in deionized water at 80 °C. The corrosion tests were conducted in 400 °C/10 MPa steam in a manner consistent with the ASTM G2/G2M-06 standard practice [12]. It specifies use of water with a deaeration practice to reduce dissolved oxygen to low levels. To validate the 14 days corrosion tests, three Zircaloy-4 Atucha I tube coupons with known performance were used as controls. A rack and several hooks made of Zircaloy-4 allow all the test samples to be hung inside the autoclave, the control coupons were placed at the top, middle and bottom of the enclosure while the alloy Zr-Nb-Ta samples were placed in the middle part. The corrosion behavior of the specimens was evaluated by measuring the weight gain as a function of the exposure time.

3. Results and discussion

3.1. The SPP precipitation/dissolution in the β-quenched alloys

The SPP´s arrangement in the alloys, after the thermal treatments of β quenching and subsequent equilibrium annealing, are showed in the optical and SEM micrographs of Figs. 1a-c. As discussed in references [9, 13], in all three alloys, the SPP´s arrangement agrees with the well-known precipitation mechanism of Zr-Nb alloys water-quenched from 1000 °C, or more, and annealed for a long time between 500 and 600 °C. The SADP from the particles in the replica is shown in Fig. 1c together with their bright and dark field images, the electron diffraction analysis confirmed that the precipitates were of the β phase (bcc).

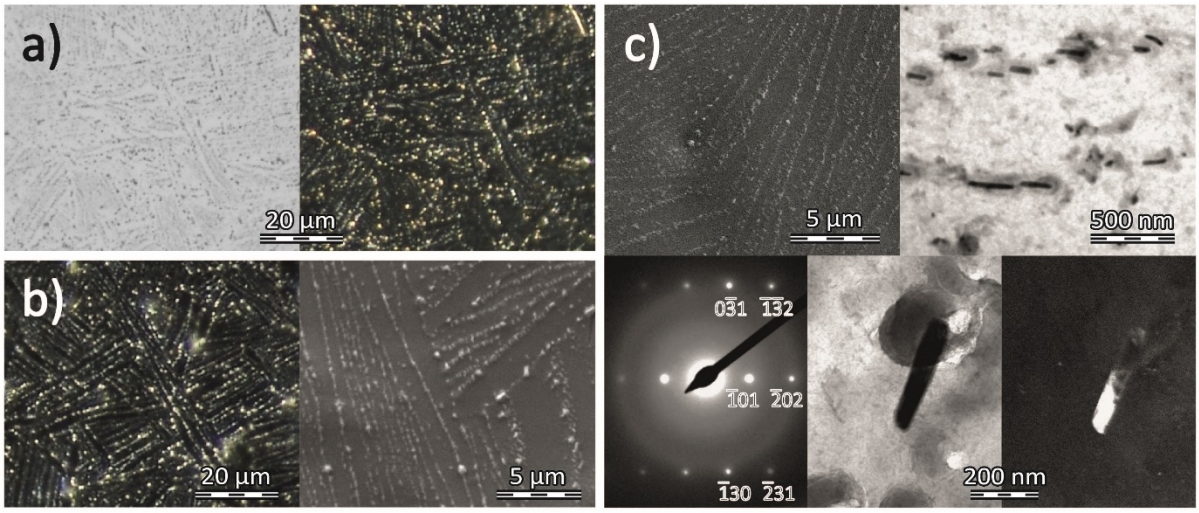

Figure 1: a) The brightfield-darkfield contrast in light microscopy of the Zr-1.05Nb alloy; b) Optical darkfield contrast and SEM micrographs of the Zr-0.85Nb-0.20Ta alloy and c) SEM micrograph of the Zr-0.85Nb-0.40Ta alloy and TEM bright field micrograph of its carbon extractive replica. In the lower part of the figure, the SAED pattern of a β particle with zone axis [313] and its bright field and [10$\bar{1}$] dark field images.

The sum of ten EDS-TEM spectra measured in the matrix α phase of the Zr-1.05Nb alloy and in the β phase precipitates (carbon replica) of the Zr-0.85Nb-0.40Ta alloy are shown in Figs. 2a and 2b, respectively. The X-ray lines necessary for the chemical quantitative analysis are highlighted in blue. Tantalum is a heavy element, and the critical ionization energy of the innermost shell (K) is too high to be reached by the voltage used in TEM. Therefore, in these

alloys it is necessary to use the family of L lines in the energy range between 9 and 10 keV to quantify Ta. Similar characterization was performed in both phases for all the alloys studied. The results are summarized in Figure 3. It seems that the Ta content in the alloy slightly reduces the solubility of Nb in the alpha phase while increasing the total solubility (Nb + Ta). As expected, Ta is a stronger β-stabilizer than Zr, it reduces the solubility of Zr but increases the total solubility in the β phase.

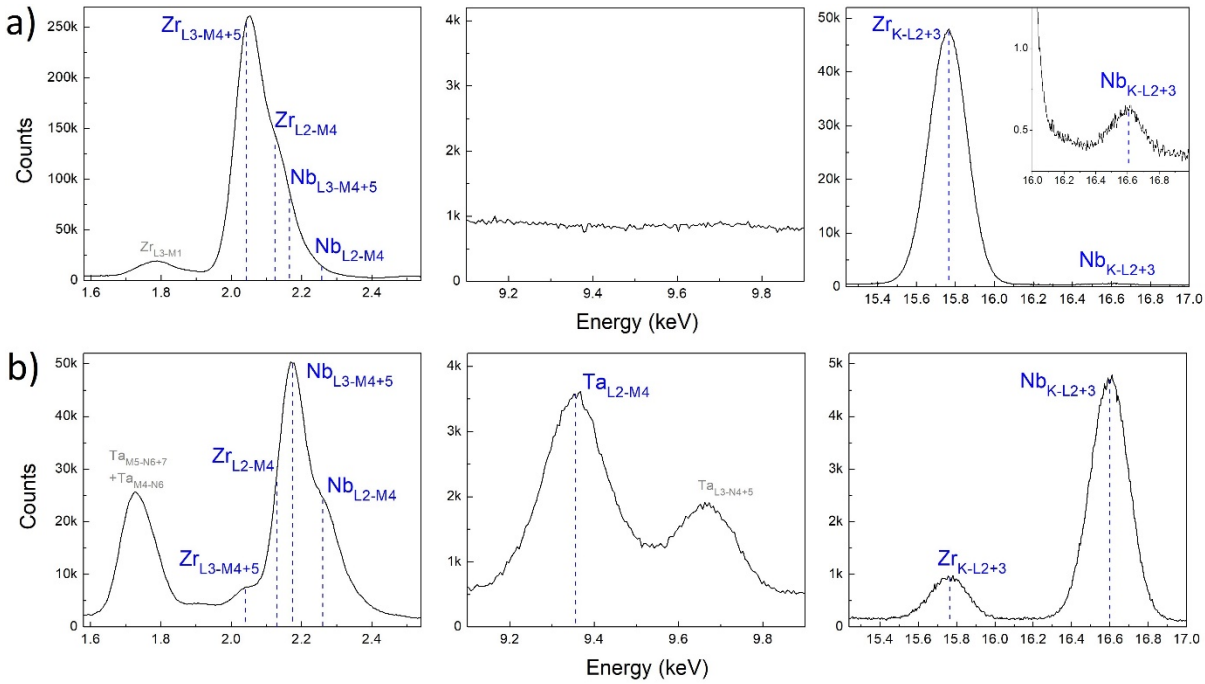

Figure 2: The key parts of the EDS-TEM spectrum for quantification of Zr, Nb and Ta in Zr-Nb alloy with tantalum addition. a) α phase of the Zr-1.05Nb alloy; b) β phase precipitate of the Zr-0.85Nb-0.40Ta alloy.

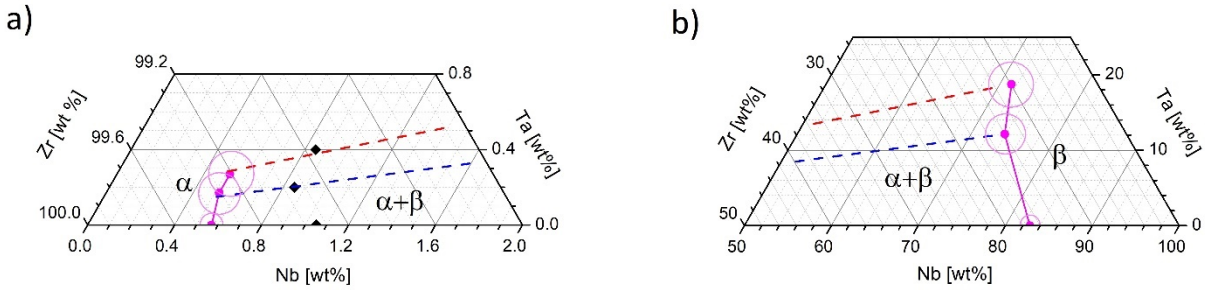

Figure 3: The zirconium (a) and niobium (b) apices of the ternary system Zr-Nb-Ta showing the nominal chemical composition of the alloy (symbols in black) and the phases (symbols in magenta) in equilibrium at 570 °C. Circles in magenta indicate the range of uncertainty in EDS-TEM measurements. Dotted lines indicate the ternary tie-lines.

The thermal analysis of the alloys is shown in Fig. 4a. To enhance clarity, we have sketched only the transformation profile zone using the base-line subtracted DSC profiles obtained on heating. Two endothermic peaks are present, the first one corresponds to the dissolution of the β_{Nb} particles and the second one corresponds to the overall allotropic transformation $\alpha_{Zr} \rightarrow \beta_{Zr}$. On cooling, not shown here, the rate of temperature change prevents the formation of the β_{Nb} precipitate and, therefore, only the peak corresponding to the allotropic transformation $\beta_{Zr} \rightarrow \alpha_{Zr}$ is observed. The modelling of the Nb-Ta-Zr ternary system was performed by Thermocalc™ (TCNI8 database) in order to compare it with our experimental results. Fig.4b shows the calculated vertical sections containing the ternary tie-lines of Fig. 3. Due to the increase in components of the alloy, the monotectic transformation of the binary system becomes a transformation that involves a three-phase equilibrium spread over a range of temperature and composition. The

starting temperature for that transformation is indicated by an arrow in each thermogram of the Fig. 4(a) and reflects an increase as the content of Ta increases. The trends of decreasing (Nb+Ta) solubility in $\beta_{Nb/Ta}$ phase (at 570 degrees) and increasing transitions temperatures with Ta addition are well represented by the TCNI8 database. In contrast, the database does not show the increase of (Nb+Ta) solubility in α_{Zr} phase.

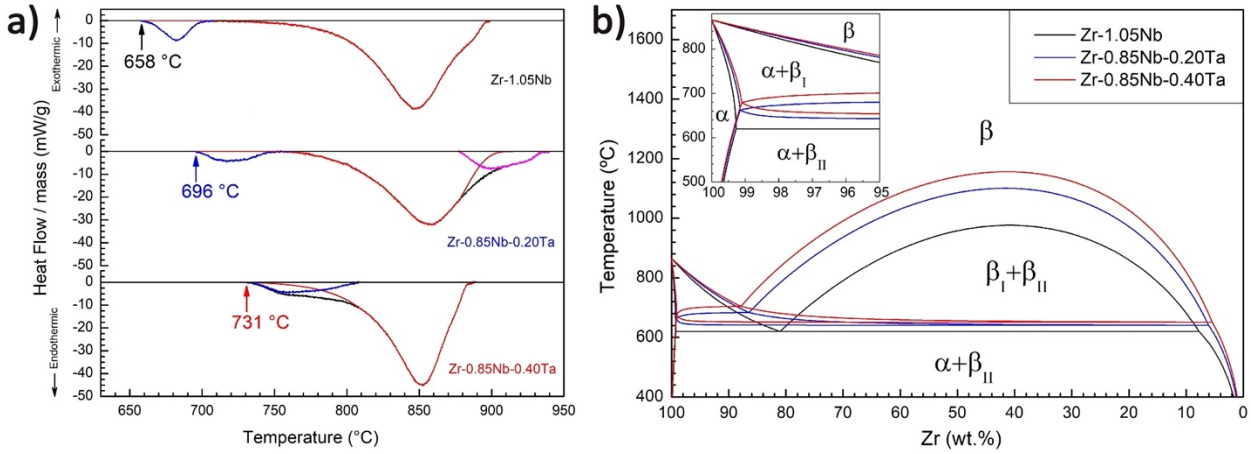

Figure 4: a) Baseline-corrected DSC curves obtained on heating of the alloys after equilibrium annealing. SPP´s dissolution peak (blue line); allotropic transformation (red line), unidentified third phase transformation (magenta line). b) Calculated vertical sections for the Nb-Ta-Zr system containing the ternary tie-lines of Fig. 3.

3.2. The SPP precipitation after hot and cold rolling steps of the β-quenched alloys.

The grains morphology of the alloys after the rolling process is shown in Fig. 5a. The average grain size was 4.4 µm which is consistent with similar values reported for commercial M5® alloy [14]. As can be seen in Fig. 5b, the SPP´s are arranged along wandering narrow bands that go through several recrystallized grains. When looking at this arrangement in more detail, as in the Fig. 5c, it is seen that a band line may have separate small precipitates if the alloy does not contain Ta or large elongated precipitates if it does.

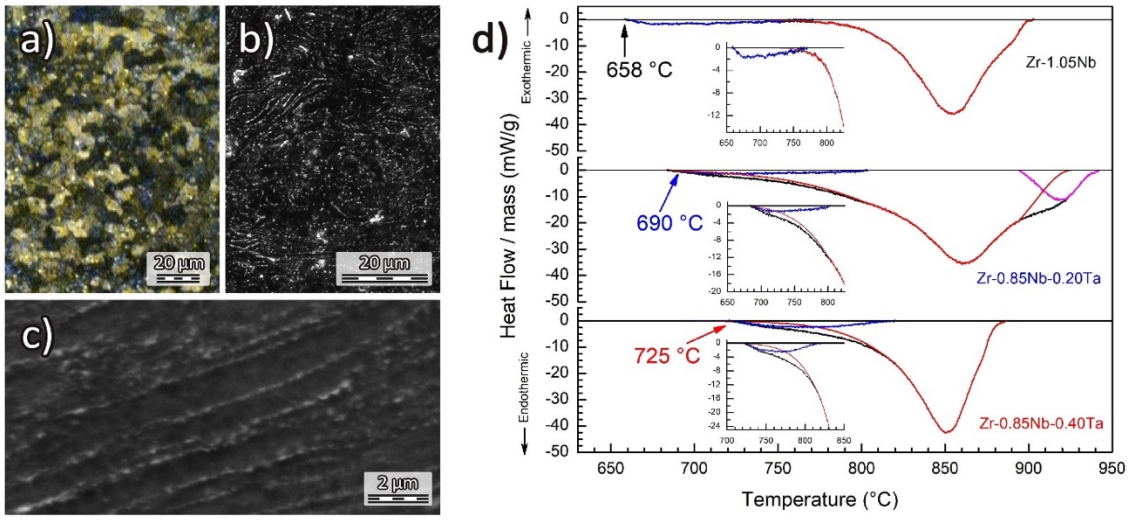

Figure 5: Polarized (a) and darkfield contrast (b) optical micrographs and SEM (c) micrograph of the Zr-0.85Nb-0.20Ta alloy after the rolling process. (d) Baseline-corrected DSC curves obtained on heating of the alloys after the rolling process. SPP´s dissolution peak (blue line); allotropic transformation (red line), unidentified third phase transformation (magenta line)

The enthalpy change, $(\Delta H/m_s)$, associate with the dissolution of the $\beta_{Nb/Ta}$ precipitates can be estimated from the area under the peak observed in the plot of the heat flux per gram of each alloy sample in Figs. 4a and 5d. Table 1 shows the experimental values obtained for the three alloys and the two thermomechanical treatments. Considering that, neglecting other minor phases, the mass fraction of $\beta_{Nb/Ta}$ particles for the alloys in thermodynamic equilibrium, $C^{eq}_{\beta_{Nb/Ta}}$, can be calculated with the data in Fig 3; then the mass fraction of $\beta_{Nb/Ta}$ particles in the rolled alloys, $C^{rolled}_{\beta_{Nb/Ta}}$, can be estimated with the following equation, $C^{rolled}_{\beta_{Nb/Ta}} = \left\{\left[\frac{\Delta H}{m_s}\right|^{rolled}\right] \Big/ \left[\frac{\Delta H}{m_s}\right|^{eq}\right]\} C^{eq}_{\beta_{Nb/Ta}}$. The estimated values for both mass fractions are also shown in Table 1.

Table 1. Mass fraction of $\beta_{Nb/Ta}$ phase from calorimetric thermograms of rolled alloys.

Alloy	$\left[\frac{\Delta H}{m_s}\right|^{eq}\right]$	$C^{eq}_{\beta_{Nb/Ta}}$	$\left[\frac{\Delta H}{m_s}\right|^{rolled}\right]$	$C^{rolled}_{\beta_{Nb/Ta}}$
	(J/g)		(J/g)	
Zr-1.05Nb	2.05 ± 0.01	0.58 ± 0.09	1.34 ± 0.17	0.38 ± 0.11
Zr-0.85Nb-0.20Ta	1.66 ± 0.12	0.45 ± 0.09	1.22 ± 0.18	0.33 ± 0.19
Zr-0.85Nb-0.40Ta	2.42 ± 0.14	0.46 ± 0.10	1.73 ± 0.12	0.33 ± 0.11

3.3. Effect of Ta addition on hydrogen solubility in Zr-1Nb

The results of the hydrogen solubility in alloy samples with the equilibrium annealing at 570 °C are summarized in Table 2. If the initial hydrogen concentration of the zirconium sponge (≈ 45 ppm) is adding to that incorporated by gaseous charging, the TSSD value of Zr-1.08Nb alloy agrees very well with that reported by Khatamian et al. [15] for Zr-1Nb alloy aged at 500 °C for 1000 h. The observed hysteresis between cool-down and heat-up TSS of Zr-1.08Nb agrees with that reported by Parodi et al. [16] in Zr-2.5Nb aged for 168 h at 500 °C. The general conclusion can be drawn that tantalum addition to Zr-1Nb alloy has a small influence. The trend of the effect with increasing Ta content shows a decrease in hydrogen solubility at low content, but then reverses this trend and increases it at higher Ta content.

Table 2. Hydride dissolution and precipitation peak temperature data measured using the DSC test on alloy samples.

Alloy	Added hydrogen (ppm)	TSSD (°C)	TSSP (°C) $Hold\ time = 10\ min$ $T_{max} = 500$°C	ΔT (°C)
Zr-1.05Nb	198.0±5.7	414.3±0.6	345.6±0.5	68.7±1.1
Zr-0.85Nb-0.20Ta	202.0±8.2	420.5±0.6	347.1±1.2	73.4±1.8
Zr-0.85Nb-0.40Ta	198.0±9.8	412.6±0.9	339.1±1.4	73.5±2.3

3.4. Behavior in short-term corrosion tests

The corrosion test carried out in this investigation is mainly used as zirconium alloys' acceptance test according to ASTM G2/G2M-06 standard, but in such a role, establishes a tolerance and, therefore, has been widely used in new alloys' development. Fig. 6 shows the effect of thermo-mechanical processing and tantalum addition on the corrosion behavior of Zr-1Nb alloys, in all cases the average corrosion behavior of Zircaloy-4 tube coupons is included.

The weight gain of the water-quenched specimens is greater than that of Zircaloy-4, except for the alloy without Ta. Our alloy samples were extracted from buttons that were water-quenched from beta phase, the cooling rate was the same for buttons with and without Ta, but Nb diffuses faster than Ta in Zr [17], therefore, the amount of Ta remaining in the supersaturated state in the matrix should be higher than the Nb. If Ta in solution is as detrimental as Nb for corrosion resistance of zirconium, the difference in behavior respect of Zircaloy-4 is largely due to the amount of Nb and Ta in the supersaturated state of the water-quenched samples, the Zircaloy-4 coupons have stabilized microstructures with their alloying elements contained mainly in precipitated particles [2,3]. This hypothesis is reinforced with the results shown in Fig. 6b, the precipitation of the $\beta_{Nb/Ta}$ phase increases the corrosion resistance in Zr-1Nb alloys with the addition of Ta beyond that observed in Zry-4. But the improvement seems to depend more on the mass fraction of the precipitated $\beta_{Nb/Ta}$ phase than the amount of Nb and Ta in the α_{Zr} phase, as can be inferred from the comparison of the results in Figs 6b and 6c. Although another factor must be considered to correlate the corrosion resistance and the mass fractions of the $\beta_{Nb/Ta}$ of the samples in thermodynamic equilibrium reported in Table 1, that is, the enthalpy of formation of the phase $\beta_{Nb/Ta}$ should increase with the Ta added to the alloy [13].

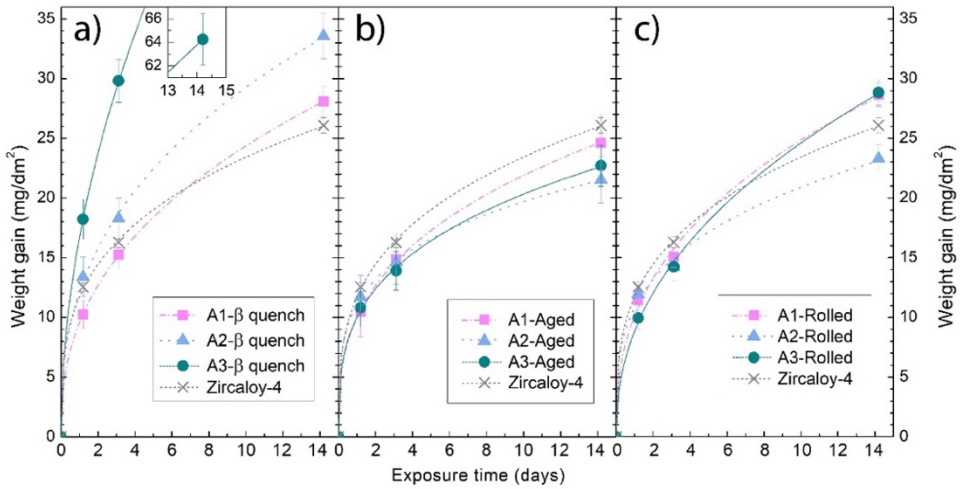

Figure 6: The effects of thermo-mechanical processing and tantalum addition on the corrosion behavior of Zr-1Nb alloys corroded at 400 °C steam for 14 days: a) Zr-1.05Nb; b) Zr-0.85Nb-0.20Ta and c) Zr-0.85Nb-0.40Ta

4. Conclusions

The $(\alpha + \beta)$ microstructure in Zr-1.05Nb, Zr-0.85Nb-0.20Ta and Zr-0.85Nb-0.40Ta (wt.%) alloys were obtained with the following two thermo mechanical processes after a water quenching from β_{Zr}: a) annealed at 570 °C for 3840 h and b) a combination of intermediate annealing temperatures and cold rolled steps. The results of the first process are the following: i) The laths of α_{Zr} phase (matrix) are decorated on boundaries by $\beta_{Nb/Ta}$ phase particles, and also inside them, with the particles aligned in parallel lines; ii) The Ta addition showed a continuous increase of solubility of (Nb+Ta) in α_{Zr} phase and a small decrease of (Zr+Ta) in the $\beta_{Nb/Ta}$ phase; and iii) The monotectoid transformation of the biphasic microstructure in the binary Zr-1Nb alloy becomes a transformation that involves a three-phase equilibrium spread over a range of temperature and composition in the ternary alloy containing Ta, the starting temperature for that transformation increases with the amount of Ta added. The second research objective adding mechanical deformation found similar results, but with the mass fraction of precipitated $\beta_{Nb/Ta}$ phase being slightly less.

The corrosion resistance of the Ta-containing Zr-1Nb experimental alloys was improved, although a slight decrease in hydrogen solubility was observed at low Ta content. Even though the corrosion resistance testing should be expanded to corroborate the outstanding trend observed at 14 days, it is worth further research on the Zr-1Nb-xTa alloy system as a candidate material for applications in the nuclear reactor core.

Acknowledgments

This study was supported by FonCyT, through PICT-2015-2267 and PICT-2018-01671 projects and by UNSAM, through PAI 2020 - 80020190200024SM project. P.A. Ferreirós & A.J. Knowles acknowledge funding from the UK Engineering and Physical Sciences Research Council (EPSRC) Grant EP/T01220X/1. The authors would also like to thank Jóhan Pauli Magnussen for his help with the phase equilibrium modelling.

References

[1] Duan Z, Yang H, Satoh Y, Murakami K, Kano S, Zhao Z, Shen J, Abe H (2017) Current status of materials development of nuclear fuel cladding tubes for light water reactors. Nuclear Engineering and Design 316:131-150. doi.org/10.1016/j.nucengdes.2017.02.031

[2] Jeong YH, Lee KO, Kim HG (2002) Correlation between microstructure and corrosion behavior of Zr-Nb binary alloy, Journal of Nuclear Materials 302(1):9-19. doi.org/10.1016/S0022-3115(02)00703-1

[3] Jeong YH, Kim HG, Kim TH (2003) Effect of β phase, precipitate and Nb-concentration in matrix on corrosion and oxide characteristics of Zr-xNb alloys. Journal of Nuclear Materials 317(1):1-12. doi.org/10.1016/S0022-3115(02)01676-8

[4] Kim HG, Jeong YH, Kim TH (2004) Effect of isothermal annealing on the corrosion behavior of Zr-xNb alloys. Journal of Nuclear Materials 326(2-3):125-131. doi.org/10.1016/j.jnucmat.2004.01.015

[5] Moorehead M, Yu Z, Borrel L, Hu J, Cai Z, Couet A (2019) Comprehensive investigation of the role of Nb on the oxidation kinetics of Zr-Nb alloys. Corrosion Science 155:173-181. doi.org/10.1016/j.corsci.2019.04.017

[6] Datta PK, Du HL, Burnell-Gray JS (2005) Corrosion of Intermetallics. In: ASM Handbook Volume 13B Corrosion: Materials 2005. ASM International, Materials Park, Ohio, p 490–512

[7] Emel'ianov VS, Godin IG, Evstiukhin AI (1958) Study of the zirconium apex of the Zr-Ta-Nb phase diagram. The Soviet Journal of Atomic Energy 4:211-220. doi.org/10.1007/BF01587180

[8] Azevedo CRF (2011) Selection of fuel cladding material for nuclear fission reactors. Engineering Failure Analysis 18(8):1943-1962. doi.org/10.1016/j.engfailanal.2011.06.010

[9] Ferreirós PA, Alonso PR, Quirós DP, Zelaya E, Rubiolo GH (2020) Accurate quantitative EDS-TEM analysis of precipitates and matrix in equilibrium (α+β) Zr–1Nb alloys with Ta addition. Journal of Alloys and Compounds 847:156372. doi.org/10.1016/j.jallcom.2020.156372

[10] Toffolon C, Brachet JC, Guilbert T, Hamon D, Urvoy S, Servant C, Charquet D, Legras L, Mardon JP (2001) Vieillissement thermique des alliages de zirconium-niobium en phase α (570 °c). Journal De Physique IV France 11(pr-1):99-108. doi.org/10.1051/jp4:2001110

[11] IAEA – TECDOC – 1609. (2009) Intercomparison of techniques for inspection and diagnostics of Heavy Water Reactor Pressures Tubes. Determination of hydrogen concentration and Blister characterization., IAEA, Vienna, Austria

[12] Standard Test Method for Corrosion Testing of Products of Zirconium, Hafnium, and Their Alloys in Water at 680 °F or in Steam at 750 °F (2011). In: ASTM G2/G2M-06, ASTM International, West Conshohocken, PA

[13] Ferreirós PA, Savoy Polack EC, Lanzani LA, Alonso PR, Quirós PD, Mieza JI, Rubiolo GH (2021) Effects of thermo-mechanical process on phase transitions, hydrogen solubility and corrosion of Ta-modified Zr-1Nb alloys. Journal of Nuclear Materials 553:153039. doi.org/10.1016/j.jnucmat.2021.153039

[14] Rautenberg M, Feaugas X, Poquillon D, Cloué JM (2012) Microstructural characterization of creep anisotropy at 673 K in the M5® alloy. Acta Materialia 60(10):4319-4327. doi.org/10.1016/j.actamat.2012.04.001

[15] Khatamian D (1999) Solubility and partitioning of hydrogen in metastable Zr-based alloys used in the nuclear industry. Journal of Alloys and Compounds 293-295:893-899. doi.org/10.1016/S0925-8388(99)00388-6

[16] Parodi SA, Ponzoni LME, De Las Heras ME, Mieza JI, Domizzi G (2016) Study of variables that affect hydrogen solubility in α + β Zr-alloys. Journal of Nuclear Materials 477:305-317. doi.org/10.1016/j.jnucmat.2016.05.027

[17] Neumann G, Tuijn C (2008) Chapter 4 Self-Diffusion and Impurity Diffusion in Group IV Metals. In: Pergamon Materials Series 2008, p 149-213. doi.org/10.1016/S1470-1804(08)00004-7